CHAPTER 4

Construction, Theory, and Practical Considerations for using Self-referencing of Ca^{2+}-Selective Microelectrodes for Monitoring Extracellular Ca^{2+} Gradients

Mark A. Messerli and Peter J. S. Smith

BioCurrents Research Center
Cellular Dynamics Program
Marine Biological Laboratory
Woods Hole, Massachusetts, USA

METHODS IN CELL BIOLOGY, VOL. 99

0091-679X/10 $35.00
DOI: 10.1016/S0091-679X(10)99004-3

Abstract

Ca^{2+} signaling in the extra- and intracellular domains is linked to Ca^{2+} transport across the plasma membrane. Noninvasive monitoring of these resulting extracellular Ca^{2+} gradients with self-referencing of Ca^{2+}-selective microelectrodes is used for studying Ca^{2+} signaling across Kingdoms. The quantitated Ca^{2+} flux enables comparison with changes to intracellular [Ca^{2+}] measured with other methods and determination of Ca^{2+} transport stoichiometry. Here, we review the construction of Ca^{2+}-selective microelectrodes, their physical characteristics, and their use in self-referencing mode to calculate Ca^{2+} flux. We also discuss potential complications when using them to measure Ca^{2+} gradients near the boundary layers of single cells and tissues.

I. Introduction

Regulation of resting $[Ca^{2+}]_i$ and the control of spatial and temporal dynamics during Ca^{2+} signaling require coordinated transport between membrane-separated compartments, giving rise to Ca^{2+} fluxes across organelles and the plasma membrane. Movement of Ca^{2+} across the plasma membrane via transporters, exchangers, or channels gives rise to minute gradients of [Ca^{2+}] in the extracellular boundary layer that reflect changes in $[Ca^{2+}]_i$. The near real-time extraction of these gradients requires a detection method that is not disturbing to the local chemical environment, functions over a wide dynamic range, and possesses high sensitivity, selectivity, and spatial resolution. For these reasons extracellular Ca^{2+} gradients have been monitored with self-referencing of Ca^{2+}-selective microelectrodes (CaSMs), enabling noninvasive characterization of Ca^{2+} transport and signaling events. Unlike most fluorescent or luminescent indicators, CaSMs were originally developed for measuring both intracellular and extracellular [Ca^{2+}] (listed in Lanter *et al.*, 1982). Measurement of minute Ca^{2+} gradients on the outside of cells was limited by electrical drift in the system. For this reason, a modulation technique was introduced (Kühtreiber and Jaffe, 1990) that enabled reduction of drift and provided a simple means for calculating Ca^{2+} flux. The method was later coined ''self-referencing'' and has been extended to other ion-selective microelectrodes and amperometric microelectrodes enabling characterization of fluxes of many different analytes (Messerli *et al.*, 2006; Smith *et al.*, 2007). Measurement of Ca^{2+} fluxes with self-referencing has enabled direct comparison of Ca^{2+} fluxes measured with other techniques including radioactive tracers, fluorescent and luminescent ion indicators, and voltage clamp. We will first discuss the construction and general properties of CaSMs before discussing their use with the self-referencing approach.

II. CaSM Construction

A. Micropipette Fabrication

Ion-selective microelectrodes are based on an ion-selective solvent or liquid membrane, immobilized in the tip of a glass micropipette with a backfilling electrolyte. The glass micropipette housings are pulled from 1.5 mm outer diameter borosilicate (TW150-4 World Precisions Instruments, Sarasota, FL), aluminosilicate (A150-100-10 Sutter Instruments, Novato, CA**),** or quartz glass (Q150-110-10, Sutter Instruments). Inner filaments, commonly used to load electrolyte solutions to the tips of micropipettes, are avoided. Although the glass body is fragile, it provides distinct advantages over other materials including low cost, excellent resistive properties necessary for use with the high-resistance liquid membranes, and easy fabrication of small tips. Micropipettes are pulled, silanized, and stored in bulk, $\sim$50 per wire rack. The glass is pulled down to a final edge slope of 0.15–0.17 and an inner tip diameter of 2–3 μm. Borosilicate and aluminosilicate micropipettes are pulled on a horizontal heated filament puller (P-97, Sutter Instruments) while quartz pipettes are pulled on a horizontal laser puller (P-2000, Sutter Instruments). Latex gloves are worn during handling of the glass before silanization.

B. Silanization

The hydrophilic glass surfaces are coated with a hydrophobic silane to enable adhesion and high electrical resistance between the glass and the hydrophobic liquid membrane. While many forms of silanization exist, we prefer vapor deposition of *N*,*N*-dimethyltrimethylsilylamine (cat# 41716 Sigma-Aldrich, St. Louis, MO) as it enables rapid and uniform coating of numerous micropipettes, simultaneously. A wire rack of micropipettes is placed in a small solid wall metal box (8 cm $\times$ 8 cm $\times$ 10 cm) with a swinging door within the oven so that the silane vapor can be trapped in a small region around the pipettes. Prior to coating, the glass is dried for 20 min at 240 °C under vacuum (28 in Hg). This shortens drying time and decreases loss of hydroxyl groups (Deyhimi and Coles, 1982; Munoz *et al*., 1983). Higher temperatures may dry glass more quickly as well; however, this silane has ignited two out of four times at $\geq$250 °C. After drying, atmospheric pressure is recovered by purging the oven with Argon. A small volume of silane (20 μL) is dropped into a tiny glass beaker in the metal enclosure and the door to the enclosure is closed before the oven door is closed. The glass is exposed to the silane vapor for 20 min before removing and placing the micropipettes in a sealed bell jar with desiccant in the bottom. Functional CaSMs have been produced from micropipettes that have been stored in this manner for up to a month. This method has reduced variation in the quality of silanization.

C. Microelectrode Construction

Standard, electrolyte-based CaSMs consist of a short column of liquid membrane ($\sim$30 μm) with a longer column of Ca^{2+} containing electrolyte (5 mm) used to make electrical contact with the voltage recording headstage via a Ag/AgCl wire. Commercially available vented pipette holders (WPI, Sarasota, FL, Warner Instruments, Hamden, CT) are used to immobilize the CaSMs while loading and recording from the high input impedance electrometers $\geq 10^{15}$ Ω (BioCurrents Research Center, Woods Hole, MA; Molecular Devices, Sunnyvale, CA; Warner Instruments, Hamden, CT). CaSMs are constructed by first backfilling a few millimeters of the electrolyte into a silanized micropipette with a long blunt needle and syringe, before tip loading the liquid membrane. The backfilling electrolyte has varied from 100 nM Ca^{2+} buffered with 5 mM EGTA, 10 mM HEPES with 90 mM KCl (Tsien and Rink, 1981) to simply 100 mM $CaCl_2$ (Kühtreiber and Jaffe, 1990). However, based on further discussion below it will be shown that the backfilling solution should be based on the bath [Ca^{2+}] with additional electrolyte, 100 mM KCl, to make electrical contact with the Ag/AgCl wire. Ca^{2+}-selective liquid membranes can be mixed in the lab or purchased premixed (cat# 21048 (ETH1001), cat# 21196 (ETH129); Sigma-Aldrich, St. Louis, MO).

Tip loading of the liquid membrane is performed under microscopic control, displayed in Fig. 1A. The electrolyte filled micropipette on the right is positioned near a loading pipette on the left, a tip broken micropipette that has been dip-loaded with liquid membrane. Both the loading pipette and the CaSM are connected to air-filled syringes with plastic tubing so that pressure can be applied. The threaded plunger (TP) syringe in Fig. 1A allows a small controlled pressure to create a small bulge of liquid membrane away from the loading pipette which aids loading of the CaSM. A plastic syringe (PS) with a three-way valve for the CaSM enables applying and venting pressure before loading and before removing the CaSM from the electrode holder. After positioning both the loading pipette and the CaSM within the field of view under the microscope objective, Fig. 1B, pressure is applied to the back of the CaSM to push the electrolyte to the tip. Pressure is vented and the tip of the CaSM is immediately positioned within the liquid membrane bulge held in the loading pipette. Surface tension will immediately draw the liquid membrane into the silanized micropipette. A combination of pressure and suction is used to achieve a liquid membrane column of the desired length ($\sim$30 μm). After the desired length is achieved, the CaSM tip is removed from the liquid membrane, the back of the CaSM is vented to atmospheric pressure, and the CaSM is removed from its holder.

III. Properties of CaSMs

A. Response to Ion Activity

The potential across the Ca^{2+}-selective liquid membrane in the tip of the CaSM is comprised of two phase boundary potentials, between the interfaces of the liquid membrane with (1) the backfilling solution and (2) the extracellular medium, and

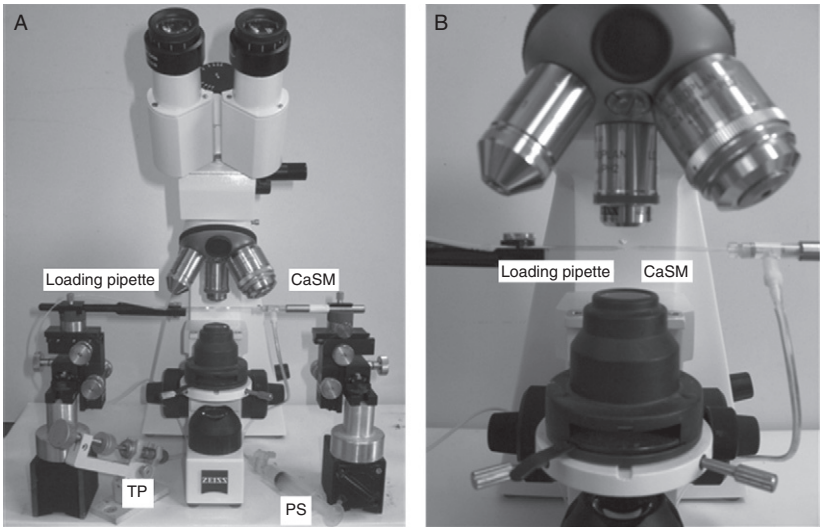

Fig. 1 Ca^{2+}-selective microelectrode tip filling station. (A) Micropositioners on each side of an upright microscope are used to position the tips of a loading pipette and a CaSM in the field of view. The stage has been removed. The threaded plunger (TP) syringe and the plastic syringe (PS) are connected to the loading pipette and CaSM via plastic tubing enabling application of pressure and suction to control the length of liquid membrane loaded into the CaSM from the loading pipette. (B) Higher magnification of A showing the close positioning of the glass loading pipette and glass CaSM. The system is mounted on a large metal plate to reduce vibration during loading.

also the diffusion potential between the two ends of the column of liquid membrane (Bakker *et al.*, 1997). The diffusion potential is considered negligible as bulk movement of Ca^{2+} across the liquid membrane does not occur during common usage with high-impedance electronics and no current flow. The inner phase boundary potential is considered constant due to the rigorous clamping of Ca^{2+} with buffers or with high concentrations of Ca^{2+} in the backfilling electrolyte. The external phase boundary potential, for an ideal ion-selective microelectrode, is related to the extracellular ion activity by the Nernst equation,

$$E = E_O + S \log a_i \quad (1)$$

where "E_o" is the sum of constant potential contributions, 'S'is the Nernstian slope = $(2.3RT)/(z_iF)$ (R, T, and F hold their standardized meanings) and "a_i" is the activity of the primary ion. Constant potential contributions are comprised of the boundary potentials and liquid junction potentials that exist across the circuit comprising the reference and measuring electrodes. The valence "z_i" of Ca^{2+} produces a slope only half as steep ($\sim$29 mV/order magnitude change in Ca^{2+}) compared to monovalent ions. The high selectivity of the two Ca^{2+} liquid membranes discussed here along with the generally standard physiological media that are used enables us to perform flux

calculations according to the Nernst equation listed above. However, in complex media with significantly interfering ions, the slope of response can be reduced. The decrease in slope can be predicted using the Nicolsky–Eisenman equation for ions of similar valence and the extended Nicolsky–Eisenman equations for ions of different valence (Bakker *et al.*, 1994). In some cases it may be more practical to perform an empirical determination of the slope of the line describing the relationship between measured voltage and the change in ionic activity. This determination is performed by making up the working medium with slightly higher and lower concentrations of Ca^{2+} and determining the slope of response. A sub-Nernstian response may reflect the presence of an interfering ion or of a substance that is fouling the microelectrode.

According to the Nernst equation, the voltage output is dependent on ionic activity. However, as ion activity is directly proportional to ion concentration, via the activity coefficient, and the changes that occur to the activity coefficient due to changes in ionic strength are negligible during self-referencing in physiological saline, we will use concentration in place of activity for further discussion.

B. Selectivity

A primary motivation for early development of CaSMs was to monitor intracellular $[Ca^{2+}]$ (Lanter *et al.*, 1982; Tsien and Rink, 1981). This required a liquid membrane with high selectivity for monitoring the low resting $[Ca^{2+}]_i$ ($\sim$100 nM) in the presence of higher concentrations of potentially interfering ions including K^+ ($\sim$120 mM), Na^+ ($\sim$10 mM) and Mg^{2+} ($\sim$1 mM). Accordingly, two different Ca^{2+} ionophores with very high selectivity were reported (Ammann *et al.*, 1975, 1987; Lanter *et al.*, 1982). Some of their selectivity coefficients for Ca^{2+} over other common cations are listed in Table I. Selectivity for Ca^{2+} over these cations is relatively good compared to liquid membranes for other ions. However, not all inorganic or organic ions have been tested and may therefore act as interferents. Not only do interfering ions reduce the electrode's voltage response to the primary ion but they also slow the response time of the electrode (Bakker *et al.*, 1997). This point is particularly important when using the electrodes in self-referencing mode where a temporal component is part of the modulation approach. In biological applications, it is critical for the investigator to empirically test the voltage response of a CaSM in the medium in which the experiments are to be performed. Simple solutions of the primary ion are not sufficient. Additionally, the CaSM should be tested for interference or fouling due to the addition of transport blockers or cellular poisons.

C. Spatial Resolution

Small, micron-sized sensors give rise to high spatial resolution. The spatial resolution is defined first by the external surface area of the Ca^{2+}-selective liquid membrane, but also by the sampling time and the distance between the source of the Ca^{2+} transport and the CaSM. This holds true for the high-impedance

Table I
Selectivity coefficients of two different Ca^{2+}-selective liquid membranes

	Selectivity coefficients ($\log {}_{CaM}{}^{Pot}$)	
Interfering ion (M)	ETH1001	ETH129[a]
K^+	−5.4[b]	−7.2
Na^+	−5.5[b]	−5.8
Mg^{2+}	−4.9[b]	−6.7
NH_4^+	−5.0[c]	−3.6
H^+	−4.4[c]	−2.5

[a]Ammann *et al.* (1987).
[b]Lanter *et al.* (1982).
[c]Ammann *et al.* (1975).

headstages $\sim 10^{15}\ \Omega$ that are typically used, which help to decrease the bulk movement of Ca^{2+} between the medium and liquid membrane. Spatial resolution is decreased due to diffusion of Ca^{2+} in the bulk medium from nearby transport events. Diffusion of Ca^{2+} from 10 to 20 μm away will reach the CaSM in only ~20 and ~80 ms, indicating that the sampled volume is much larger than the immediate dimensions of the CaSM tip. As these events are diffusing from regions further away, the local concentration change that they produce near the tip of the CaSM will be much smaller (proportional to $1/r^2$) than the signals from events immediately in front of the CaSM. The decay in signal with distance is evident from measurements of extracellular K^+ gradients due to efflux through single K^+ channels (Messerli *et al.*, 2009). The sampling domain of the CaSM is therefore slightly larger than the surface area of the liquid membrane and decays rapidly with increasing distance from the surface.

D. Response Time

Self-referencing of CaSMs requires the use of CaSMs with relatively short response times so that the CaSM can reach equilibrium in a short period of time at its new position. The response time of CaSMs is governed by the ability to provide charge to the sensing node. In an ideal measuring system, diffusion through the unstirred layer at the surface of the electrode defines the response time of the sensors when the liquid membrane is equilibrated with the salt of an ion to which the electrode responds (Bakker *et al.*, 1997). For ion-selective microelectrodes, this process may occur so quickly that the electronics of the system slow the measured response (Ammann, 1986). Low input impedance of the amplifier and parasitic capacitances in the circuit will draw more charge than an ideal system therefore slowing the response time of the system. Amplifier input impedances of

Table II
CaSMs based on ionophore ETH1001 possess short response times in physiological saline over a range of [Ca^{2+}]

Response times ($t_{95\%}$ ms)			
0.1–1 mM	1–10 mM	10–1 mM	1–0.1 mM
48 ± 7	53 ± 10	58 ± 9	81 ± 10

Physiological saline consists of (in micromolar) 120 NaCl, 5 KCl, 2 $MgCl_2$, 10 HEPES with the $CaCl_2$ concentration listed above. CaSMs remained stationary during the experiment, while three adjacent streams of media (1 mL/min) were rapidly positioned (< 8 ms) in front of the measuring electrode. These measurements describe the response time of the entire measuring system for 4 CaSMs.

$\geq 10^6$ GΩ are typically used to accommodate ion-selective microelectrodes that have high resistances, 1–20 GΩ (Ammann, 1986). Even with the best electronics, the time constant (RC, resistance times capacitance) of the CaSM itself imposes a low pass filter. Resistance is primarily dependent on the tip diameter and length of the column of liquid membrane and capacitance is primarily dependent on the thickness and dielectric constant of the wall of the glass micropipette. To reduce the resistance of the CaSMs, they are fabricated with relatively large tips of 2–3 μm inner diameter and with short columns of liquid membrane ~30 μm. The short columns are achieved by tip loading the liquid membrane as discussed above. Capacitance can be lowered by using thicker walled borosilicate glass (1.5 mm O. D. 0.84 mm I.D. cat# 1B150-6, WPI Sarasota, FL). The construction design listed above has produced CaSMs with response times shorter than 100 ms, Table II. In practice, a slight deviation from the expected length does not change the response time very much, at least when considering the use of these electrodes in the self-referencing application.

IV. Self-referencing of CaSMs

A. Differential Concentration Measurement

Self-referencing of CaSMs was developed to measure extracellular Ca^{2+} gradients/currents that may have existed near previously characterized extracellular voltage gradients (Kühtreiber and Jaffe, 1990). For example, relatively steady efflux of Ca^{2+} across the plasma membrane gives rise to a gradient of Ca^{2+} with a higher concentration near the cell. Self-referencing of CaSMs is implemented by measuring the [Ca^{2+}] at two points in that Ca^{2+} gradient. The electrical variation of a single CaSM due to thermal noise, ±100–200 μV, of the high-impedance sensors and chemical drift is too large to enable measurement of such small differences in extracellular Ca^{2+}. As a result, a frequency sensitive method of

detection was explored based on response times of about 1 s reported for CaSMs commonly used at that time (Ammann, 1986). The general measuring protocol includes intermittent collection of ion concentration by a single CaSM at a position near the biological preparation and then at a position some distance away orthogonal to the source. A CaSM is shown in Fig. 2A and B at the two positions, next to a mouse pancreatic islet. The excursion distance in this case is 20 μm but can vary between 5 and 50 μm depending on the size of the cell or cellular preparation. At each pole of excursion, the CaSM is allowed to reach equilibrium (~0.25 s) before recording the average local ion concentration for about 1 s. Considering that the CaSMs possess response times of less than 0.1 s, 0.25 s is plenty of time to reach equilibrium. The CaSM is then immediately positioned to the opposite pole, and allowed to reach equilibrium before recording the local ion concentration. The movement of the CaSM between the two positions is controlled by stepper motors set to move the sensor at a rate of 40 μm/s such that it takes 0.25 s to reach its new

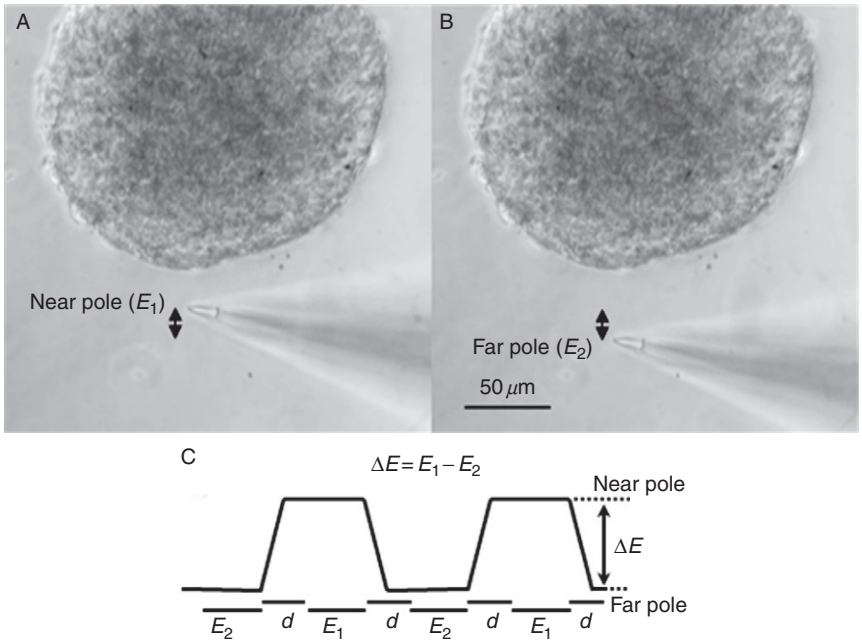

Fig. 2 Ca^{2+} flux measurements performed with self-referencing of a Ca^{2+}-selective microelectrode near a mouse pancreatic islet. (A) In the near pole the CaSM collects the average [Ca^{2+}]-dependent potential for 1 s, E_1. (B) After movement to the far pole and equilibration, the average [Ca^{2+}]-dependent potential is collected again for 1 s, E_2. (C) Data collection scheme portraying Ca^{2+} efflux. The automated determination of the differential [Ca^{2+}]-dependent potential, ΔE, is used to determine Ca^{2+} flux. This measuring scheme continues, as defined by the user. The [Ca^{2+}]-dependent potential is discarded, (d), during periods of movement (~0.25 s) and during equilibration in the new position (~0.25 s).

position. A differential concentration recording between the two poles of excursion is collected, about every 3 s. The measurement scheme continues until stopped by the user. The differential recording possesses peak to peak noise of ± 10 μV while longer periods of signal collection and averaging can enable extraction of concentration differences that give rise to 1 μV differences or a 0.008% difference from the background [Ca^{2+}]. Figure 2C illustrates this collection scheme during Ca^{2+} efflux where E_1 and E_2 are the recorded ion concentration–dependent potentials at the two poles. The recording collected during movement and equilibration at the new pole is discarded, labeled "*d*" in Fig. 2C. A differential Ca^{2+} measurement is collected over a period of about 3 s, which is faster than the low frequency drift, thus reducing its influence on the measurement. Signal averaging at each pole over a period of 1 s reduces the influence of the high frequency noise. Measurement of the differential ion concentration–dependent voltage, ΔE, between the two positions over time enables further enhancement of the signal-to-noise ratio.

This modulation approach was termed self-referencing, referring to the fact that the measurements, collected by a single CaSM, are compared to each other in order to determine the concentration difference between the two points. The signal collected by a single CaSM at one point in space and time is referenced to the signal collected by that same CaSM at a different point in space and time in order to reduce electrical drift of the measuring system. The CaSM has its own bath reference electrode. While this differential measurement could be achieved with two similar, CaSMs, positioned at known distances from the source, the sensitivity would suffer from the signal drift and noise inherent to two separate measuring systems.

Measured differential voltages of ± 10s μV are extracted from relatively large offset potentials ± 100s mV by using a combination of amplification methods. Low gain must be used with the large offset potentials in order to keep the signal within the dynamic range of the amplifier. As a result, low resolution digital systems will not be able to register small changes in the differential voltage. A 12-bit system with a dynamic range of ± 10 V provides only 4.9 mV/bit resolution while a 16-bit system provides only 0.3 mV/bit. Additional amplification prior to digitization is necessary to resolve signals at or below 1 μV. Two separate methods for amplification are used; (1) a nearly equal and opposite electrical offset is supplied before amplification (sample hold mode) and (2) a running average of the low gain measurement is subtracted from the real-time input before amplification (RC subtract mode). Sample hold mode applies a known voltage that is selected either manually or automatically from the signal after a set duration of time to null the offset potential before applying 10^3 times gain. The primary disadvantage for this mode is that drift can take the system back out of the dynamic range of the amplifier so that a new potential must be applied regularly. The advantage is that it does not need an additional correction factor to compensate for the signal lost due to the filtering that occurs in RC subtract mode. In RC subtract mode, a high-pass filter is used to collect a running average potential that is subtracted from the potentials collected in the near and far pole. The signals are then amplified

10^3 times before digitizing. Typically, this mode employs a high-pass filter with a time constant of 10 s. RC subtract allows amplification for systems with large drift but involves a correction factor to offset the high-pass filter. The correction factor will be dependent on the time constant of the high-pass filter and the period of data acquisition. For standard conditions, a period of 3.3 s (0.3 Hz translation frequency), 40 μm/s translation speed, 10 s time constant of the high-pass filter along with data selection of the last 70% of the half cycle, we calculate that the signal is 7% smaller than a square wave with similar rise time.

Automated, repetitive positioning of the CaSMs is controlled by three stepper motors arranged in an X, Y, Z configuration with the Z plane parallel to the plane of the stage of the microscope. Smooth linear motion is obtained by coupling each of the stepper motors to a lead screw controlling the position of three small translational plates connected together to form a three-dimensional positioner (BioCurrents Research Center, Woods Hole, MA). Low voltage control of the stepper motors prevents electrical feedback to the high-impedance headstage of the CaSM. Positioning can be achieved over a working distance of 3–4 cm with submicron resolution and repeatability (Danuser, 1999). A computer interface enables repetitive motion and positional control with the Faraday cage closed.

B. Differential Concentration Determination

The relationship between the measured differential voltage and the differential ion concentration between the two poles of excursion for an ideal CaSM can be determined using the Nernst equation.

$$\begin{aligned} E_1 - E_2 &= (E_O + S\log C_i)_1 - (E_O + S\log C_i)_2 \\ \Delta E &= (S\log C_i)_1 - (S\log C_i)_2 \\ \Delta E &= \log C_{i(1)}^{S_1} - \log C_{i(2)}^{S_2} \\ \Delta E &= \log\left(\frac{C_{i(1)}^{S_1}}{C_{i(2)}^{S_2}}\right) \end{aligned} \tag{2}$$

"E_1", "$C_{i(1)}$", and "S_1" are the measured voltage, $[Ca^{2+}]$ and slope of the voltage–$\log(C_i)$ graph for the near pole of excursion. The subscript 2 labels the same parameters for the far pole of excursion. The slow changing constant potential contributions "E_o" are reduced if not eliminated by calculating the difference between potentials over short periods of time.

Equation (2) enables a clear picture of the relationship of the sensitivity of detection to the background ion concentration during measurements. For a given $[Ca^{2+}]$ change due to cellular flux, the concentration in the position next to the cell, $C_{i(1)}$, is the sum of the background ion concentration and the concentration change generated by the source while $C_{i(2)}$, in most cases, is close to the background ion concentration. It is easier to generate a larger ΔE when the background concentration of the measured ion is lower as the ratio of $C_{i(1)}/C_{i(2)}$

will be much larger/smaller for the same Ca^{2+} efflux/influx on lowered background $[Ca^{2+}]$. This has led to the lowering of the background $[Ca^{2+}]$ in order to generate ΔE with a greater signal-to-noise ratio, see Table IV. Care must be taken to ensure that changing the background concentration does not interfere with normal cellular activity.

Rearrangement of Eq. (2) relates the $[Ca^{2+}]$ in the near pole of excursion to the $[Ca^{2+}]$ at the far pole of excursion.

$$C_{i(1)} = C_{i(2)}^{\frac{S_2}{S_1}} \times 10^{\frac{\Delta E}{S1}} \tag{3}$$

For an ideal electrode, the voltage output is close to the Nernstian slope over a wide range of $[Ca^{2+}]$ so $S_1 = S_2 = S = \frac{2.3RT}{z_i F}$. Therefore, Eq. (3) simplifies to

$$C_{i(1)} = C_{i(2)} \times 10^{\frac{\Delta E}{S}} \tag{4}$$

For minute fluxes that are typically measured with self-referencing, the average concentration of Ca^{2+} at the far pole, position 2, is not too different from the average concentration of Ca^{2+} in the bulk solution. Therefore the difference in $[Ca^{2+}]$ between the two points of excursion can be described as follows:

$$\Delta C = C_{i(1)} - C_{i(2)} = C_{bath} \times 10^{\frac{\Delta E}{S}} - C_{bath} \tag{5}$$

A primary assumption here is that the excursion distance is small compared to the extent that the gradient extends out into the bulk solution so that the concentration difference between the two excursion points is linear. For minute gradients measured from small cells ($\sim$10 μm diameter), an excursion of 10 μm will most likely sample over a distance in which the concentration difference is not linear and therefore will lead the investigator to underestimate the true flux. Incorrect estimation of the true flux could also occur during a two-point measurement in a more intense, extended gradient, where the concentration of the ion in the far pole is substantially different from the background concentration of the ion. In both of these cases, a three-point measurement should be performed in order to (1) more carefully map the concentration gradient with a third point to ensure a linear relationship or determine a more accurate nonlinear relationship and (2) to determine the concentrations in the gradient relative to the background concentration of the ion in the bath.

The selectivity of Ca^{2+} liquid membranes is relatively good compared to liquid membranes for other ions. Therefore, measurement of Ca^{2+} gradients in the presence of a constant concentration of an interfering ion or in the presence of a gradient of an interfering ion is not a major concern. However, specific circumstances may require the use of higher concentration of an interfering ion and the two cases need to be addressed. Details necessary to account for these situations have been addressed previously (Messerli *et al.*, 2006; Smith *et al.*, 2007).

C. Calculation of Flux

The differential concentration measurement is converted to flux to provide a direct representation of the number of ions passing through a unit area per unit time. Calculation of flux enables comparison of Ca^{2+} transport between different systems as it takes into account the diffusion coefficient of Ca^{2+}, the distance over which the differential concentration measurement was acquired, the surface geometry of the source, and the distance of measurement from the source. It also provides a value for comparison of Ca^{2+} flux measured with self-referencing of CaSMs to other methods for monitoring Ca^{2+} including intracellular fluorescent and luminescent ion indicators and radioactive tracer flux studies. For planar sources where the measuring electrode is relatively close to a large source, such as a tissue, sheet of cells or large diameter cell, and the differential concentration is measured over a small distance "Δx" within the gradient next to the source, flux (J) is

$$J = -D\frac{\Delta C}{\Delta x} \tag{6}$$

where "D" is the diffusion coefficient of Ca^{2+}. By this model, at equilibrium the flux measured at some distance from the source is the same as the flux at the surface of the source. According to this equation, efflux, a higher concentration of Ca^{2+} near the source, is identified by a negative flux.

In order to determine flux at the cell surface for known surface geometries, it is useful to calculate analyte flow, that is, the quantity of substance (Q) moving per unit time (Henriksen *et al.*, 1992). Flow is the same for all concentric surfaces surrounding the source surface. Flux at the source surface is the flow divided by the surface area of the source. Therefore, radially emanating flow from a cylindrical surface is

$$\text{Flow} = \frac{Q}{t} = -\frac{2\pi D}{\ln(b/a)}(\Delta C) \tag{7}$$

where "D" is the diffusion coefficient of the analyte and "a" and "b" are the radial distances between the center of the cylinder and the electrode tip at the near and far poles, respectively. These equations have been adapted from Crank (1967). Analyte flux at the surface of the cylinder is then determined by dividing by its surface area $2\pi rl$. A caveat of this approach is the assumption that the flow is equal at all points around the cylinder and along the shaft of the cylinder. An alternative is to calculate flux per unit length by dividing by $2\pi r$ (Henriksen *et al.*, 1992).

The flow from a spherical source is

$$\text{Flow} = \frac{Q}{t} = -4\pi D\frac{ab}{b-a}(\Delta C) \tag{8}$$

Flux at the cell surface can then be determined by dividing by the spherical surface area $4\pi r^2$.

D. Correction for Ca^{2+} Buffering

The presence of Ca^{2+} buffers or binding agents with the appropriate affinity can lead to collapse of Ca^{2+} gradients by shuttle buffering (Speksnijder *et al.*, 1989). Ca^{2+} can diffuse from the surface of the cell in either its free state or bound to the buffer. CaSMs only measure the free concentration of Ca^{2+}. The actual Ca^{2+} flux at a source is the sum of the measured free Ca^{2+} flux and the unmeasured Ca^{2+} flux diffusing as Ca^{2+} bound to buffer.

$$J_{\text{Ca\_total}} = J_{\text{Ca\_measured}} + J_{\text{Ca\_Buffer}} \tag{9}$$

Knowing the conditions under which the Ca^{2+} flux was measured including the $[Ca^{2+}]$ of medium, dissociation constant, K_d, of the buffers and concentration of the buffers present, a simple relationship can be derived to determine the ratio of Ca^{2+} diffusing bound to buffer compared to the freely diffusing Ca^{2+}. Shuttle buffering of H^+ is a bigger concern than for Ca^{2+} due to the larger number of H^+ buffers that are used in physiological media. The equations that exist to correct for shuttle buffering of H^+ (Messerli *et al.*, 2006; Smith *et al.*, 2007) can be adapted for use with Ca^{2+} flux correction and may be necessary under specific circumstances.

$$x_i = \frac{D_B}{D_{Ca^{2+}}}[B]\frac{K_d}{\left(K_d + [Ca^{2+}]\right)^2} \tag{10}$$

The correction factor, "x_i", is the ratio of the Ca^{2+} bound buffer flux to the free Ca^{2+} flux. Therefore

$$J_{\text{Ca\_total}} = J_{\text{Ca\_measured}}(1 + x_i + \cdots + x_n) \tag{11}$$

where a number of different Ca^{2+} buffers ($x_i + \cdots + x_n$) may be collapsing the Ca^{2+} gradient. The correction factor is based on three criteria, the ratio of the diffusion coefficients of the Ca^{2+}-buffer complex to free Ca^{2+}, the Ca^{2+} buffer concentration, and the dissociation constant, K_d, of the Ca^{2+} buffer compared to the $[Ca^{2+}]$ of the medium. The K_d is the inverse of the more commonly used "stability constant" also known as the association constant. Only Ca^{2+} buffers/binding agents that have K_d values near the range of the extracellular $[Ca^{2+}]$ will act as effective shuttle buffers during self-referencing of CaSMs. Table III lists a few of these compounds. Note that two of the compounds, ADA and Bicine, are commonly used as H^+ buffers. Generally, the Ca^{2+} K_d values of other Good buffers are not in the range of normal extracellular $[Ca^{2+}]$ or are very poor Ca^{2+} chelators (Dawson *et al.*, 1986).

E. Measurement of Voltage Gradients

The use of CaSMs with self-referencing is subject to a similar problem that occurs with the use of intracellular CaSMs; specifically they detect not only changes in ion concentration but also voltage. Extracellular voltage gradients

Table III
List of Ca^{2+} binding compounds that can act as shuttle buffers for extracellular Ca^{2+} in the 0.1–1.0 mM range

Ligand	$\log(K_d)$
Pyrophosphate	−5.0
N-(2-acetamido)iminodiacetic acid (ADA)	−4.0[1]
ATP	−3.8
Citric acid	−3.5
Oxalic acid	−3.0
Polyphosphate	−3.0
N,N-bis(hydroxyethyl)-glycine (Bicine)	−2.8

Values were obtained from Dawson *et al.* (1986) except as noted [1](Lance *et al.*, 1983).

have been mapped near many different systems (Borgens *et al.*, 1989; Nuccitelli, 1986) Extracellular electric fields generated by cells are generally very small especially in high conductivity media such as animal saline. However, in lower conductivity saline ion transport can give rise to relatively large electric fields >1 μV/10 μm which can be detected with self-referencing microelectrodes. Plants for example, drive transcellular currents through them, as a result of ion transport across single cells or tissues. In low conductivity medium, these currents generate substantial voltage gradients next to the cells, coexisting with the concentration gradients of the transported ions. The differential voltage measured by the CaSM will be the sum of the voltage differences due to the $[Ca^{2+}]$ difference and the voltage difference. For example, a peak voltage difference during oscillating current influx of about 9 μV would occur over a 10-μm distance immediately in front of a lily pollen tube. Peak current density around 0.4 $\mu A/cm^2$ was measured at a distance of about 20 μm from the cell surface with a medium resistivity of about 5000 Ω cm (Messerli and Robinson, 1998). This voltage difference is just above the background noise of the system used at that time, ± 5 μV for Ca^{2+}, (Messerli *et al.*, 1999). The voltage signals detected by the self-referencing CaSM peaked about six times larger than the differential voltage due to current flux indicating that the extracellular electric field could have contributed to the calculated Ca^{2+} flux by up to 15%.

F. Positional Artifacts

Self-referencing of CaSMs near solid objects can generate position dependent artifacts. Movement of Ca^{2+} across the external interface between the liquid membrane and bathing medium may occur through current driven and zero net current mechanisms (Bakker and Meyerhoff, 2000). Release of Ca^{2+} by the CaSM restricts its sensitivity in bulk medium by leading to a modification of the local ion

concentration at the tip of the microelectrode. During self-referencing, when the CaSM is positioned near a solid object, released Ca^{2+} can accumulate between the CaSM and the object in a short period of time leading to an artificially higher concentration of Ca^{2+} in the constrained space. Likewise, uptake of Ca^{2+} by the CaSM can lead to a depletion of Ca^{2+} in the constrained space. These artifacts are most apparent in solutions of low background [Ca^{2+}]. Figure 3 shows examples of both extremes where CaSMs are self-referenced near a 100-μm diameter glass bead. The CaSM is moving in a path so that the plane of its tip is always parallel to the near surface of the bead to enable the ISM to get closer to the surface. The ion trapping effect is reduced when the path of excursion orients the plane of the tip of the CaSM perpendicular to the near surface of the solid object, as shown in Fig. 2A and B, because the liquid membrane surface cannot get as close to the solid object. Efflux of Ca^{2+} from the microelectrode tip occurs when constructed with 100 mM $CaCl_2$ backfilling solution, originally performed by Kühtreiber and Jaffe (1990). Accumulation of the released Ca^{2+} in less than 1 s can be detected when the bath [Ca^{2+}] is 50 μM but not when it is 2 mM, giving rise to an artificial efflux of Ca^{2+} from the solid glass bead. Reducing the concentration of the primary ion in the backfilling solution is one method of reducing the ion leak (Bakker and Meyerhoff, 2000). However, when used with self-referencing this can lead to an artifact of the opposite polarity shown in Fig. 3. The CaSM constructed with

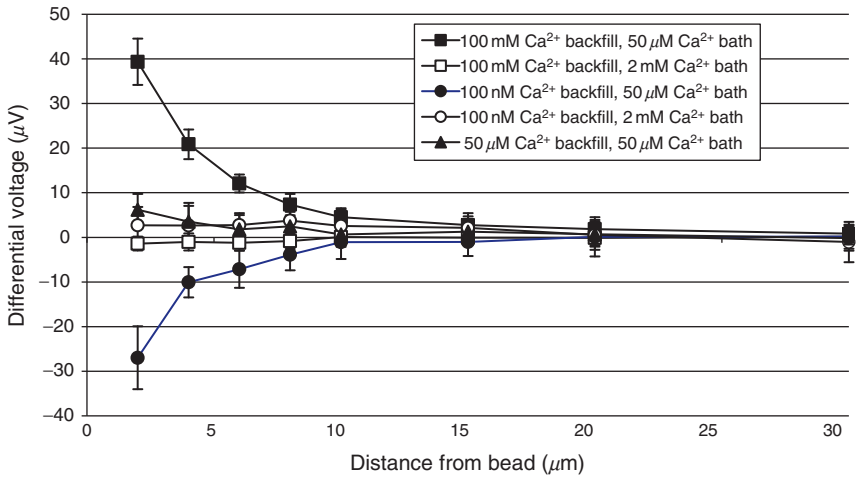

Fig. 3 Ca^{2+} movement across the tip of a CaSM can be detected in low background [Ca^{2+}] near a solid object. Electroneutral exchange of Ca^{2+} out of the tip of a CaSM (filled box) or into the tip of the CaSM (filled circle) can give rise to accumulation or depletion of the local [Ca^{2+}] between a solid object and the tip of the CaSM. In higher bath [Ca^{2+}] (empty box, empty circle) the accumulation or depletion is insignificant compared to the background [Ca^{2+}] and is therefore not detected. In lowered bath [Ca^{2+}] careful balancing of the backfilling [Ca^{2+}] with the bath [Ca^{2+}] can reduce (filled triangle) if not eliminate net movement of Ca^{2+} across the liquid membrane.

100 nM Ca^{2+} in the backfilling solution generates an influx of Ca^{2+} into the CaSM tip, depleting the local [Ca^{2+}] in the bath and giving rise to an artificial Ca^{2+} influx into the glass bead. Again this can be detected in the 50 μM Ca^{2+} solution but not the 2 mM Ca^{2+} containing bath solution. The artifact can be reduced by matching the backfilling [Ca^{2+}] with the [Ca^{2+}] in the bath. Other methods for eliminating Ca^{2+} flux across the tip of the CaSM include current clamping (Lindner *et al.*, 1999; Pergel *et al.*, 2001), or using the solid contact ion-selective electrode design (Lindner and Gyurcsányi, 2009).

V. Ca^{2+} Flux Measurements

Extracellular Ca^{2+} flux measurements have been performed on a number of different systems some of which are listed in Table IV, ranging from animal neurons and muscle to tip growing root hairs, pollen tubes, and fungi. Measured Ca^{2+} fluxes are relatively small ranging between 0.1 and 10 pmol cm^{-2} s^{-1} encouraging measurements from cells in reduced background [Ca^{2+}] $\leq$0.1 mM. The limit of flux sensitivity for a typical self-referencing CaSM with $\pm$10 μV near real-time variation performed in 1 mM bath [Ca^{2+}] is about $\pm$6.3 pmol cm^{-2} s^{-1}, an order of magnitude higher than in 0.1 mM bath [Ca^{2+}]. Considering the large transplasma membrane electrochemical driving force on Ca^{2+}, reduction of extracellular [Ca^{2+}] by an order of magnitude did not cause noticeable problems for the different preparations, at least over the few hour period during which measurements were acquired as noted by multiple authors listed in Table IV.

While efflux of Ca^{2+} in cells at rest is expected to be relatively small, the measured influx of Ca^{2+}, presumably through channels, is also relatively small. Active single 0.5 pS Ca^{2+} channels at a density of 1 μm^{-2} should give rise to a Ca^{2+} influx of about 47 pmol cm^{-2} s^{-1}. Although as noted by Hille (2001) voltage-gated Ca^{2+} channels exist at low density and low open probabilities (<0.1) even with strong depolarizing potentials indicating that low channel density and activity is sufficient to account for measured changes in $[Ca^{2+}]_i$. The channel density and activity used above may be overestimates of actual Ca^{2+} channel density. Also, weak influx may also be a result of the Ca^{2+} amplification cascades that exist to release Ca^{2+} from intracellular stores after influx through the plasma membrane.

Additional directions for the use of self-referencing with CaSMs include the study of electroneutral Ca^{2+} transporters/exchangers and extracellular Ca^{2+} signaling (Breitwieser, 2008). Ca^{2+} selective microelectrodes have been instrumental in providing the sensitivity for defining the complex transport of the Na^+/Ca^{2+} exchanger (Kang and Hilgemann, 2004) and the P-type plasma membrane Ca^{2+} pump (PMCA) in neurons (Thomas, 2009). With self-referencing of ion-selective microelectrodes, transport stoichiometries could be determined noninvasively from the outside of intact cells.

Table IV
Calcium flux measurements acquired from preparations representing multiple Kingdoms

Preparation	Ca^{2+} flux (pmol cm^{-2} s^{-1})	Conditions	Bath [Ca^{2+}] (mM)	Reference
Aplysia californica bag cell	−1 to −5	Rest, H_2O_2	0.1	Duthie *et al.* (1994)
	−1 to −5	Rest, thapsigargin	None added (0.5 mM EGTA)	Knox *et al.* (1996)
Rana catesbeiana hair cell	−0.5	Rest	0.05	Yamoah *et al.* (1998)
	+5.0	Stimulated		
Callinectes sapidus olfaction	−2.5	15% ASW[a]	0.1	Gleeson *et al.* (2000b)
	−4.0	AFW[b]	0.1	Gleeson *et al.* (2000a)
Sclerodactyla briareus smooth muscle	−1.0 to −4.0	Rest, Ach.[c]	0.1	Devlin and Smith (1996)
	−1 to −7.5	Muscarinic agonists	0.1	Devlin *et al.* (2003)
Busycon canaliculatum cardiac muscle	−1 to −4	Rest, FMRFamide	0.1	Devlin (1996)
Mouse ova	−0.02	Rest	0.05	Pepperell *et al.* (1999)
	+0.6	Bepridil addition[d]		
	±0.2	Replenished Na^+		
	+0.08 to +0.35	Addition of EGF[e]	None added	Hill *et al.* (1999)
Lilium longiflorum pollen tubes	+2 to +20	Germination	0.1	Pierson *et al.* (1994)
	+5 to +38[f]	Oscillating tip growth	0.13	Messerli *et al.* (1999)
Root hairs	+4.3 to +7.2 (alfalfa)	Tip growth, nod factor	Not listed	Herrmann and Felle (1995)
	+2.5 (*S. alba*)	Tip growth	0.1	
	+0.07 to +1.2 (*A. thaliana*)	Osmotic regulation	0.1	Lew (1998)
Neurospora crassa hyphae	−0.1	Voltage dependence	0.05	Lew (2007)
	+0.1 to +1.5	Osmotic regulation	0.05	Lew and Levina (2007)
Ceratopteris richardii spores	−3.5 top	Gravity sensing	0.02–0.05	Chatterjee *et al.* (2000)
	+0.5 bottom			
Physcomitrella patens filaments	+1–3	Gravity sensing	0.1	Allen *et al.* (2003)

[a]Artificial seawater.
[b]Artificial freshwater.
[c]Acetylcholine.
[d]Bepridil was added to block the plasma membrane Na^+/Ca^{2+} exchanger.
[e]Epidermal growth factor.
[f]Calculated flux at cell surface.

Acknowledgments

The BioCurrents Research Center is funded by NIH:NCRR grant P41 RR001395.

References

Allen, N. S., Chattaraj, P., Collings, D., and Johannes, E. (2003). Gravisensing: Ionic responses, cytoskeleton and amyloplast behavior. *Adv. Space Res.* **32**(8), 1631–1637.

Ammann, D. (1986). Ion-Selective Microelectrodes. Springer-Verlag, Berlin.

Ammann, D., Güggi, M., Pretsch, E., and Simon, W. (1975). Improved calcium ion-selective electrode based on a neutral carrier. *Anal. Lett.* **8**(10), 709–720.

Ammann, D., Bührer, T., Schefer, U., Müller, M., and Simon, W. (1987). Intracellular neutral carrier-based Ca^{2+} microelectrode with subnanomolar detection limit. *Pflügers Arch. Eur. J. Physiol.* **409,** 223–228.

Bakker, E., and Meyerhoff, M. E. (2000). Ionophore-based membrane electrodes: New analytical concepts and non-classical response mechanisms. *Anal. Chim. Acta* **416,** 121–137.

Bakker, E., Meruva, R. K., Pretsch, E., and Meyerhoff, M. E. (1994). Selectivity of polymer membrane-based ion-selective electrodes: Self-consistent model describing the potentiometric response in mixed ion solutions of different charge. *Anal. Chem.* **66,** 3021–3030.

Bakker, E., Bühlmann, P., and Pretsch, E. (1997). Carrier-based ion-selective electrodes and bulk optodes. 1. General characteristics. *Chem. Rev.* **97,** 3083–3132.

Borgens, R. B., Robinson, K. R., Vanable, J. W. J., and McGinnis, M. E. (1989). Electric Fields in Vertebrate Repair. Alan R. Liss, Inc., New York.

Breitwieser, G. E. (2008). Extracellular calcium as an integrator of tissue function. *Int. J. Biochem. Cell Biol.* **40,** 1467–1480.

Chatterjee, A., Porterfield, D. M., Smith, P. J. S., and Roux, S. J. (2000). Gravity-directed calcium current in germinating spores of *Ceratopteris richardii*. *Planta* **210,** 607–610.

Crank, J. (1967). The Mathematics of Diffusion. Oxford University Press, London.

Danuser, G. (1999). Photogrammetric calibration of a stereo light microscope. *J. Microsc.* **193,** 62–83.

Dawson, R. M. C., Elliott, D. C., Elliott, W. H., and Jones, K. M. (1986). Data for Biochemical Research. Oxford University Press, Oxford.

Devlin, C. L. (1996). A vibrating Ca^{2+}-selective electrode measures Ca^{2+} flux induced by the neuropeptide FMRFamide in a gastropod ventricle. *Comp. Biochem. Physiol.* **116A**(2), 93–100.

Devlin, C. L., and Smith, P. J. S. (1996). A non-invasive vibrating calcium-selective electrode measures acetycholine-induced calcium flux across the sarcolemma of a smooth muscle. *J. Comp. Physiol.* **166,** 270–277.

Devlin, C. L., Amole, W., Anderson, S., and Shea, K. (2003). Muscarinic acetylcholine receptor compounds alter net Ca^{2+} flux and contractility in an invertebrate smooth muscle. *Invert. Neurosci.* **5,** 9–17.

Deyhimi, F., and Coles, J. A. (1982). Rapid silyation of a glass surface: Choice of reagent and effect of experimental parameters on hydrophobicity. *Helv. Chim. Acta* **65,** 1752–1759.

Duthie, G. G., Shipley, A., and Smith, P. J. S. (1994). Use of a vibrating electrode to measure changes in calcium fluxes across the cell membranes of oxidatively challenged *Aplysia* nerve cells. *Free Rad. Res.* **20**(5), 307–313.

Gleeson, R. A., Hammar, K., and Smith, P. J. S. (2000a). Sustaining olfaction at low salinities: Mapping ion flux associated with the olfactory sensilla of the blue crab *Callinectes sapidus*. *J. Exp. Biol.* **203,** 3145–3152.

Gleeson, R. A., McDowell, L. M., Aldrich, H. C., Hammar, K., and Smith, P. J. S. (2000b). Sustaining olfaction at low salinities: Evidence for a paracellular route of ion movement from the hemolymph to the sensillar lymph in the olfactory sensilla of the blue crab *Callinectes sapidus*. *Cell Tissue Res.* **301,** 423–431.

Henriksen, G. H., Raman, D. R., Walker, L. P., and Spanswick, R. M. (1992). Measurement of net fluxes of ammonium and nitrate at the surface of barley roots using ion-selective microelectrodes. *Plant Physiol.* **99,** 734–747.

Herrmann, A., and Felle, H. (1995). Tip growth in rooth hair cells of *Sinapis alba* L.: Significance of internal and external Ca^{2+} and pH. *New Phytol.* **129,** 523–533.

Hill, J. L., Hammar, K., Smith, P. J. S., and Gross, D. J. (1999). Stage-dependent effects of epidermal growth factor on Ca^{2+} efflux in mouse oocytes. *Mol. Reprod. Dev.* **53,** 244–253.

Hille, B. (2001). Ion Channels of Excitable Membranes. Sinauer Associates, Inc., Sunderland.

Kang, T. M., and Hilgemann, D. W. (2004). Multiple transport modes of the cardiac Na^{+}/Ca^{2+} exchanger. *Nature* **427,** 544–548.

Knox, R. J., Jonas, E. A., Kao, L.-S., Smith, P. J. S., Connor, J. A., and Kaczmarek, L. K. (1996). Ca^{2+} influx and activation of a cation current are coupled to intracellular Ca^{2+} release in peptidergic neurons of *Aplysia californica*. *J. Physiol.* **494**(3), 627–639.

Kühtreiber, W. M., and Jaffe, L. F. (1990). Detection of extracellular calcium gradients with a calcium-specific vibrating electrode. *J. Cell Biol.* **110,** 1565–1573.

Lance, E. A., Rhodes, C. W., III, and Nakon, R. (1983). Free metal ion depletion by "Good's" buffers. *Anal. Biochem.* **133,** 492–501.

Lanter, F., Steiner, R. A., Ammann, D., and Simon, W. (1982). Critical evaluation of the applicability of neutral carrier-based calcium selective microelectrodes. *Anal. Chim. Acta* **135,** 51–59.

Lew, R. R. (1998). Immediate and steady state extracellular ionic fluxes of growing *Arabidopsis thaliana* root hairs under hyperosmotic and hypoosmotic conditions. *Physiol. Plant.* **104,** 397–404.

Lew, R. R. (2007). Ionic currents and ion fluxes in *Neurospora crassa* hyphae. *J. Exp. Bot.* **58**(12), 3475–3481.

Lew, R. R., and Levina, N. N. (2007). Turgor regulation in the osmosensitive cut mutant of *Neurospora crassa*. *Microbiology* **153,** 1530–1537.

Lindner, E., and Gyurcsányi, R. E. (2009). Quality control criteriz for solid-contact, solvent polymeric membrane ion-selective electrodes. *J. Solid State Electrochem.* **13,** 51–68.

Lindner, E., Gyurcsányi, R. E., and Buck, R. P. (1999). Tailored transport through ion-selective membranes for improved detection limits and selectivity coefficients. *Electroanalysis* **11,** 695–702.

Messerli, M. A., and Robinson, K. R. (1998). Cytoplasmic acidification and current influx follow growth pulses of *Lilium longiflorum* pollen tubes. *Plant J.* **16,** 87–91.

Messerli, M. A., Danuser, G., and Robinson, K. R. (1999). Pulsatile influxes of H^{+}, K^{+} and Ca^{2+} lag growth pulses of *Lilium longiflorum* pollen tubes. *J. Cell Sci.* **112,** 1497–1509.

Messerli, M. A., Robinson, K. R., and Smith, P. J. S. (2006). Electrochemical sensor applications to the study of molecular physiology and analyte flux in plants. *In* "Plant Electrophysiology," (A. G. Volkov, ed.), pp. 73–107. Springer, Berlin, Heidelberg, New York.

Messerli, M. A., Collis, L. P., and Smith, P. J. S. (2009). Ion trapping with fast response, ion-selective microelectrodes enhances detection of extracellular ion channel gradients. *Biophys. J.* **96,** 1597–1605.

Munoz, J.-L., Deyhimi, F., and Coles, J. A. (1983). Silanization of glass in the making of ion-sensitive microelectrodes. *J. Neurosci. Methods* **8,** 231–247.

Nuccitelli, R. (ed.) (1986). Ionic currents in development. Progress in Clinical and Biological Research. Alan R. Liss, Inc, New York.

Pepperell, J. R., Kommineni, K., Buradagunta, S., Smith, P. J. S., and Keefe, D. L. (1999). Transmembrane regulation of intracellular calcium by a plasma membrane sodium/calcium exchanger in mouse ova. *Biol. Reprod.* **60,** 1137–1143.

Pergel, E., Gyurcsányi, R. E., Toth, K., and Lindner, E. (2001). Picomolar detection limits with current-polarized Pb^{2+} ion-selective membranes. *Anal. Chem.* **22,** 509–514.

Pierson, E. S., Miller, D. D., Callaham, D. A., Shipley, A., Rivers, B. A., Cresti, M., and Hepler, P. K. (1994). Pollen tube growth is coupled to the extracellular calcium ion flux and the intracellular calcium gradient: Effect of BAPTA-type buffers and hypertonic media. *Plant Cell* **6,** 1815–1828.

Smith, P. J. S., Sanger, R. H., and Messerli, M. A. (2007). Principles, development and applications of self-referencing electrochemical microelectrodes to the determination of fluxes at cell membranes. *In* "Electrochemical Methods for Neuroscience," (A. C. Michael, and L. M. Borland, eds.), pp. 373–405. CRC Press, Boca Raton.

Speksnijder, J. E., Miller, A. L., Weisenseel, M. H., Chen, T. H., and Jaffe, L. F. (1989). Calcium buffer injections block fucoid egg development by facilitating calcium diffusion. *Proc. Natl. Acad. Sci. USA* **86,** 6607–6611.

Thomas, R. C. (2009). The plasma membrane calcium ATPase (PMCA) of neurones is electroneutral and exchanges 2 H^+ for each Ca^{2+} or Ba^{2+} ion extruded. *J. Physiol.* **587,** 315–327.

Tsien, R. Y., and Rink, T. J. (1981). Ca2+-selective electrodes: A novel PVC-gelled neutral carrier mixture compared with other currently available sensors. *J. Neurosci. Methods* **4,** 73–86.

Yamoah, E. N., Lumpkin, E. A., Dumont, R. A., Smith, P. J. S., Hudspeth, A. J., and Gillespie, P. G. (1998). Plasma membrane Ca^{2+}-ATPase extrudes Ca^{2+} from hair cell stereocilia. *J. Neurosci.* **18**(2), 610–624.